Available online at www.sciencedirect.com
SCIENCE DIRECT®
Journal of Electroanalytical Chemistry 559 (2003) 155–163
Journal of Electroanalytical Chemistry
www.elsevier.com/locate/jelechem

Effect of gravitational strength on nucleation phenomena of electrodeposited copper onto a TiN substrate

M. Morisue [a], Y. Fukunaka [a,*], E. Kusaka [a], R. Ishii [a], K. Kuribayashi [b]

[a] Department of Energy Science and Technology, Kyoto University, Sakyo-ku, Kyoto 606-2501, Japan
[b] Institute of Space and Astronautical Science, Yunodai, Sagamihara 229-0022, Japan

Received 3 May 2003; received in revised form 21 July 2003; accepted 29 August 2003

Abstract

Cu^{2+} ion was electrodeposited potentiostatically in 0.05 M $CuSO_4$ aqueous solutions onto a foreign substrate of TiN film sputtered on a stainless steel sheet. The amount of electricity was limited to 31.8 mC cm^{-2}, which corresponds to a 10 nm thick film, deposited uniformly without any void formation. Two different electrolytic cell configurations were designed in order to discuss quantitatively the effect of gravitational strength on the nucleation and growth of metal electrodeposition in detail: (a) a horizontal cathode surface facing downward over an anode (C/A) and (2) an anode over cathode (A/C). SEM pictures show that the nucleus number density varies from 10^7 to 10^{10} cm^{-2} depending on the negative overpotential and that the A/C configuration introduces more number of nuclei than the case of C/A at a constant overpotential. The gravitational level certainly influences the initial stage of electrodeposition of Cu^{2+} ion in $CuSO_4$ aqueous solution. Image analysis techniques further demonstrate that copper metal does not nucleate randomly over the TiN substrate, but the presence of a nucleation inhibition or exclusion zone was suggested. Thus, the growth rate of the inhibited zone should be influenced by the gravitational field vector.

Keywords: Copper electrodeposition; Nucleation phenomena; Gravitational strength; Nucleation phenomena; TiN substrate; Inhibition zone; Electrolytic cell configuration; Terrestrial experiment

1. Introduction

Non-equilibrium electrochemical interfacial phenomena are a very important topic from the aspect of energy conversion and storage technology in the operation of the International Space Station [1–10]. Unique characteristics caused by the gravitational strength difference may be expected. No systematic research has been reported, although NASA has been engaged in such an operation for more than 40 years.

Electrodeposition in microgravity (μ-*G*: 10^{-6} G–10^{-4} G where *G* is the gravitational acceleration) may also provide an example. In our first trial, copper was electrodeposited around the lateral surface of a 100 μm high copper disc cathode in a quasi-two dimensional electrolytic cell in the drop tower at Kamisunagawa, Japan [11]. The maximal duration period of electrodeposition under microgravity was limited only to 8 s. Because the magnitude of the Rayleigh number is quite small in this electrolytic cell design, it was expected that a macroscopic natural convection would not be induced even in the terrestrial experiment. The grain size of copper electrodeposited under μ-*G* was, however, apparently larger than that under 1-*G* [12]. It was not easy to reproduce the lateral surface condition of copper disc with such a thickness or height of 100 μm.

Cu^{2+} ion was then galvanostatically or potentiostatically electrodeposited on a well electropolished polycrystalline copper substrate installed in three different electrolytic cell configurations [13,14]: (a) a horizontal

* Corresponding author. Tel.: +81-75-753-5415; fax: +81-75-753-4719.
E-mail address: fukunaka@energy.kyoto-u.ac.jp (Y. Fukunaka).

0022-0728/03/$ - see front matter © 2003 Elsevier B.V. All rights reserved.
doi:10.1016/S0022-0728(03)00519-9

cathode facing downward over an anode (C/A), (b) an anode over a cathode (A/C) under 1-G and (c) that under microgravity (μ-G). Bernard type natural convection is induced in the A/C configuration, while no macroscopic natural convection is expected in the C/A configuration even in the normal gravity environment. No natural convection occurs, of course, in a microgravity environment. The C/A configuration therefore simulates the ionic mass transfer rate under microgravity. Larger grains were observed under C/A than A/C and much larger grains were, surprisingly, observed under μ-G than C/A in 1-G. This gravitational effect was observed even in the samples electrodeposited only for 2 s.

The simultaneous measurements of the ionic mass transfer and momentum transfer rate accompanying the transient electrolysis was engaged when the circuit was spontaneously closed. The momentum transfer of electrolyte is induced more slowly than the ionic mass transfer rate, because of a relatively larger inertia of electrolyte [15]. The induction of micro-scale convection within such a short duration of electrodeposition in the terrestrial experiment hardly influences the cathode surface concentration. Why were such morphological variations induced by the different levels of gravitational acceleration? The relationship may be understood between the initial stage of electrodeposition or the nucleation and growth phenomena and the shape evolution on a micro-scale.

It is however difficult to analyze the nucleation phenomena quantitatively when copper is electrodeposited on polycrystalline copper, because the nucleus and the substrate are indistinguishable from each other. Our previous studies were limited to only qualitative discussion on the crystal grain sizes [12–14].

Advances in interconnection technology have, by the way, played a key role in allowing continued improvements in integrated circuit density, performance, and cost [16,17]. The large improvements in cost and scalability can be achieved electrochemically by forming dual-damascene monolithic studs/wires, when the predictive model of shape evolution around a cavity frequently immersed in the jet or centrifugal convection flow is established. The coupling phenomena between the ionic mass transfer rate and the shape evolution have been discussed [18–20]. Deeper understanding of such a coupling phenomenon becomes indispensable in designing a micro-reactor system as well as in the microelectronics fabrication. Much faster nucleation phenomena must be expected in the semiconductor fabrication field such as ultra large-scale integration in microelectronics (ULSI) technology. Quantitative research is necessary to understand these nucleation phenomena.

This paper describes copper electrodeposition onto a TiN substrate. Through quantitative estimations of the nucleation phenomena, we will propose that this experimental system is an appropriate system to investigate the effect of gravitational strength on the nucleation related phenomena.

2. Experimental

Copper was electrodeposited potentiostatically in 0.05 M $CuSO_4$ solution on a TiN substrate using a cavity-type electrolytic cell. 100–200 nm thick TiN film was sputtered on a stainless sheet (Tigold Co. Ltd.). The electrolytic cell is illustrated schematically in Fig. 1. The effective cathode surface was limited to a circle with a 2 mm diameter by insulating a polycrystalline copper substrate with a silicon rubber sheet. The perforated anode with a 20 mm diameter was made of copper foil. A Teflon coated copper wire 0.5 mm in diameter was utilized as a conventional reference electrode. Its edge was placed perpendicularly 3 mm away from the cathode surface. 0.05 M $CuSO_4$ aqueous solutions were adjusted with high-grade copper sulfate (Nacalai Tesque Inc.). Prior to each experiment, the TiN substrates were cleaned ultrasonically and sequentially in acetone, methanol and distilled water for 15 min. The electrolyte was then deaerated for 2 h by bubbling nitrogen gas.

The electrolytic cell was arranged in two different configurations: (1) a horizontally installed cathode surface facing downward over a horizontal anode (C/A), and (2) an anode over a cathode (A/C). In the C/A configuration, the less concentrated and lighter electrolyte solution remained adjacent to the downward facing cathode surface. The gradient of the electrolyte density profile thus becomes parallel to the gravitational field vector.

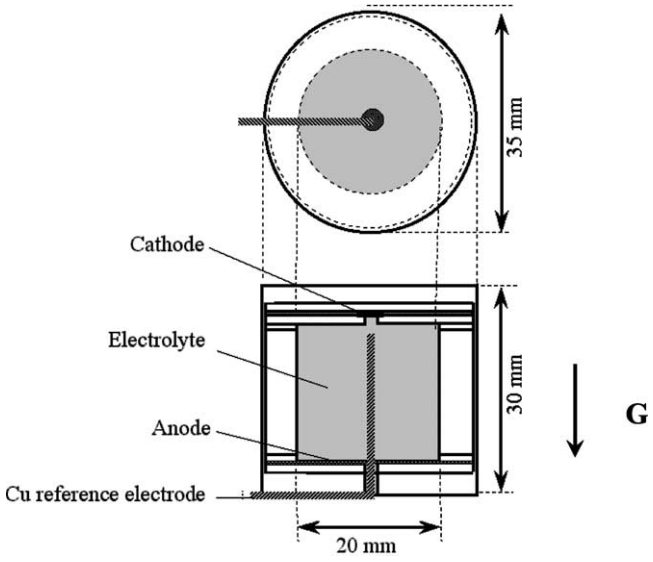

Fig. 1. Schematic illustration of a cavity-type electrolytic cell (C/A configuration).

The amount of electricity was controlled by a coulomb meter (Hokuto Denko Co. Ltd). The growth process of copper nucleus electrodeposited on TiN substrate was recorded in scanning electron microscopy (SEM) pictures. The image analysis technique was applied for the quantitive measurement using the computer software, Image-Pro PLUS 2.0 (Media Cybernetics). The nucleation related phenomena or the morphological variations during the initial stage of electrodeposition caused by the two different kinds of electrolytic cell configuration of A/C and C/A were compared.

3. Result and discussion

3.1. Time dependence of nucleus number density

Potentiostatic electrodeposition was conducted at various overpotentials, maintaining the amount of electricity constant. In order to characterize the morphological variation of the electrodeposited copper film surface with the gravitational strength level as well as the electrolytic conditions, the time dependence of the number of electrodeposited crystal grains must be examined first.

Fig. 2 demonstrates the growth process of copper grains electrodeposited at -0.5 V vs. a Cu conventional reference electrode in the C/A configuration. The duration times of electrodeposition were 4, 16, and 32 s. Copper grains were randomly precipitated on the TiN substrate, although the detailed image analysis indicates precipitated grains varying from 50 to 400 nm in size. The precipitated grain number densities determined from SEM images are 9.8×10^8, 6.8×10^8 and 7.5×10^8 cm^{-2}, for 4, 16 and 32 s respectively. The value is 9.3×10^8 cm^{-2} at 8 s, although this SEM image is not illustrated in Fig. 2. The time dependence of the grain number density is weaker than that caused by the overpotential η or by the gravitational strength inherent to the different electrolytic cell configurations, as will be described. These SEM images suggest that each precipitate corresponds to a nucleus. Henceforth, the precipitate number density may be regarded as the nucleus number density.

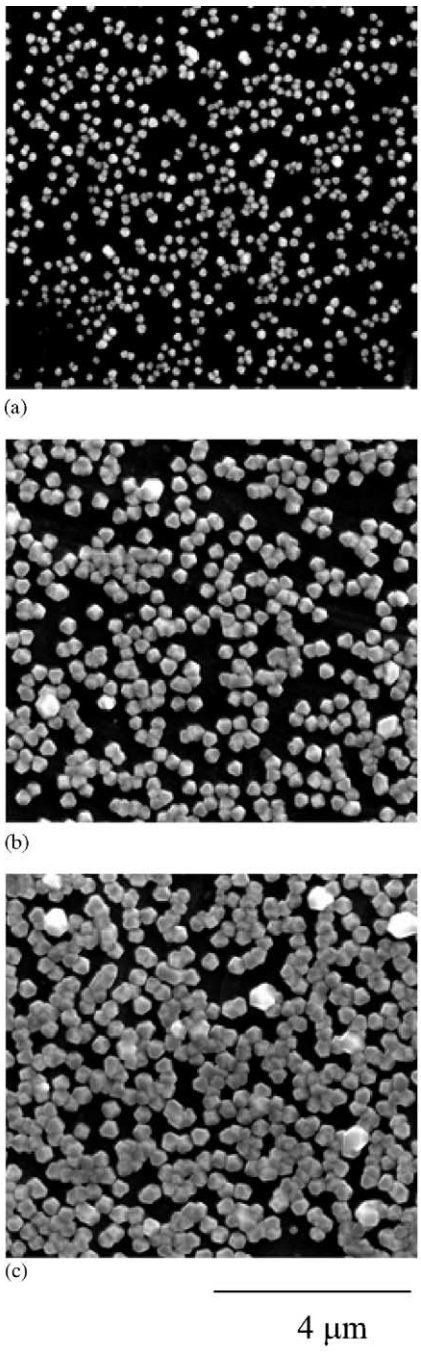

Fig. 2. SEM images of copper precipitates on the TiN substrate at -0.5 V vs. Cu for (a) 4 s, (b) 16 s, and (c) 32 s.

3.2. η and the configuration dependence of nucleus density

Cu^{2+} ion was electrodeposited on TiN at various overpotentials η vs. a $Cu \mid Cu^{2+}$ reference electrode in each cell configuration, C/A and A/C. In all experiments, the amount of electricity was set at 31.8 mC cm^{-2}. This would correspond to a 10 nm thick copper film, if it were uniformly precipitated without any void formation. Fig. 3 shows SEM images of copper precipitates electrodeposited on a TiN substrate. The images in the upper row are the samples electrodeposited in the C/A configuration and those in the lower are in the A/C configuration. The nuclei density increases with increase in the overpotential. It is emphasized that a greater number of nuclei were apparently obtained in A/C than in C/A.

Fig. 4 shows the overpotential dependence of the nuclei number densities obtained from 8.14×8.14 μm SEM images. The nuclei number densities are in the

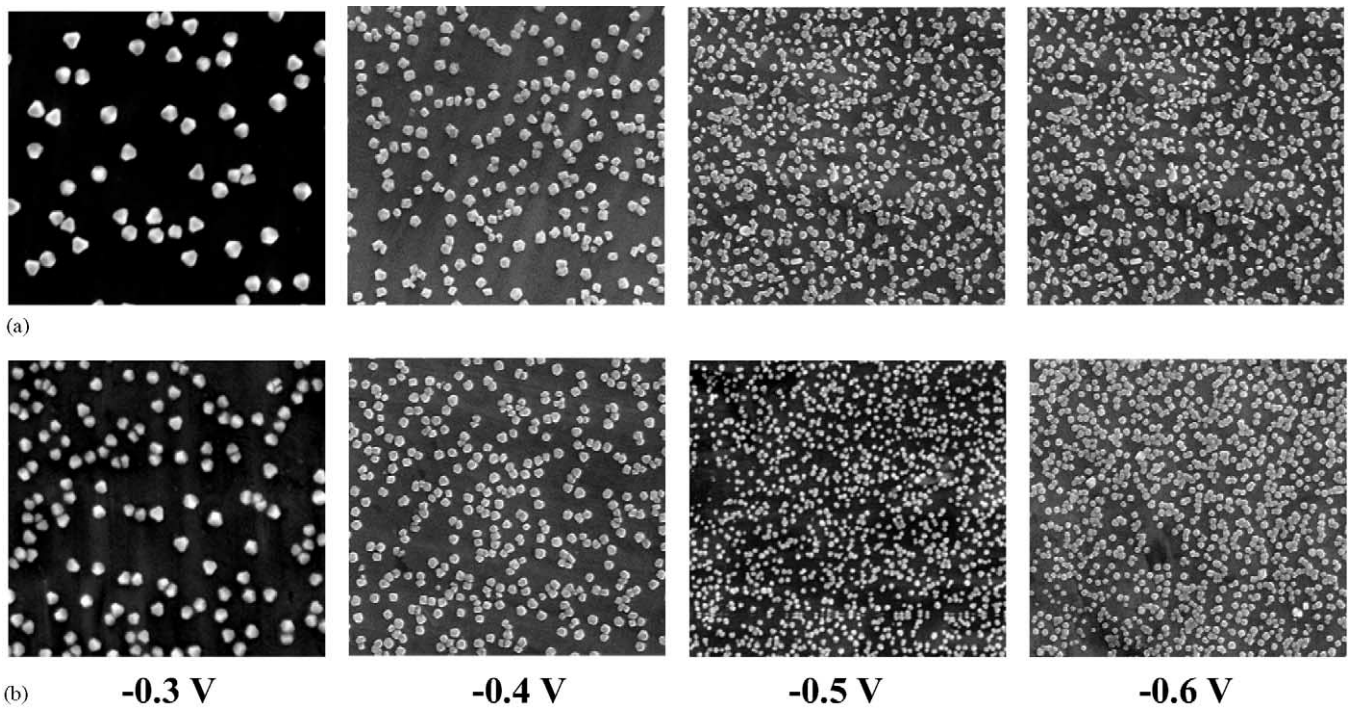

Fig. 3. 8.14 × 8.14 μm SEM images of copper precipitates on TiN substrate at various overpotentials; (a) C/A and (b) A/C.

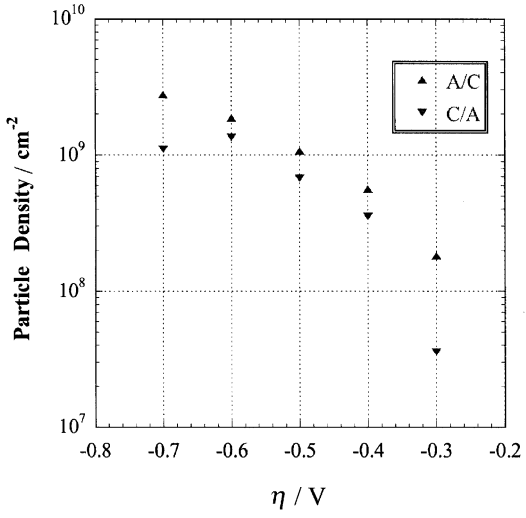

Fig. 4. Particles density vs. overpotential. The values were determined in 8.14 × 8.14 μm SEM images.

range of 10^7 to 10^{10} cm^{-2}. An exponential dependence of the nucleus number density on potential was recognized as expected. Nuclei number densities in the A/C configuration are indeed higher than in C/A over a wide range of overpotential.

Fig. 5 shows the grain size distribution determined from the SEM images. These diameters are defined under the presumption that all electrodeposited grains are hemispherical. The diameter was measured every 5° around the center of gravity in each grain in order to calculate the average diameter over 72 values. The average diameters are: $d_{mean} = 230$ nm at -0.4 V in C/A, $d_{mean} = 151$ nm at -0.6 V in C/A, $d_{mean} = 215$ nm at -0.4 V in A/C, $d_{mean} = 145$ nm at -0.6 V in A/C. A larger grain size of copper was obtained with the C/A configuration than that with A/C for a constant amount of electricity, because a lower nucleus number density was obtained with the C/A configuration than with A/C.

Fig. 6 (top) and (bottom) shows a series of current transients for the potential steps from the open-circuit potential to deposition potentials varying from -0.3 to -0.7 V: (a) in C/A and (b) in A/C. Each transient curve is characterized by a rapid decrease of current over the initial 0.5–2 s (Stage I). The instantaneous current variation in the very initial period of Stage I should correspond to charging up the double layer. No significant difference of transient current is observed between the two configurations of C/A and A/C in Stage I. This is followed by the appearance of a current density recovery with an extreme value around 2–5 s (Stage II). The extreme value is recorded for a longer duration in A/C than in C/A. No extreme value appears at -0.3 V for either electrolytic cell configuration after 40 s. The over-potential corresponding to this potential of -0.3 V is too low for the ionic mass transfer resistance to control the electrodeposition process. The current transient curves at less than -0.5 V apparently fluctuate 10–20 s after starting the electrolysis experiments in the A/C configuration (Stage III).

Bernard type natural convection should be inevitably induced with time progression in the A/C configuration under normal gravity. The fluctuating characteristics in

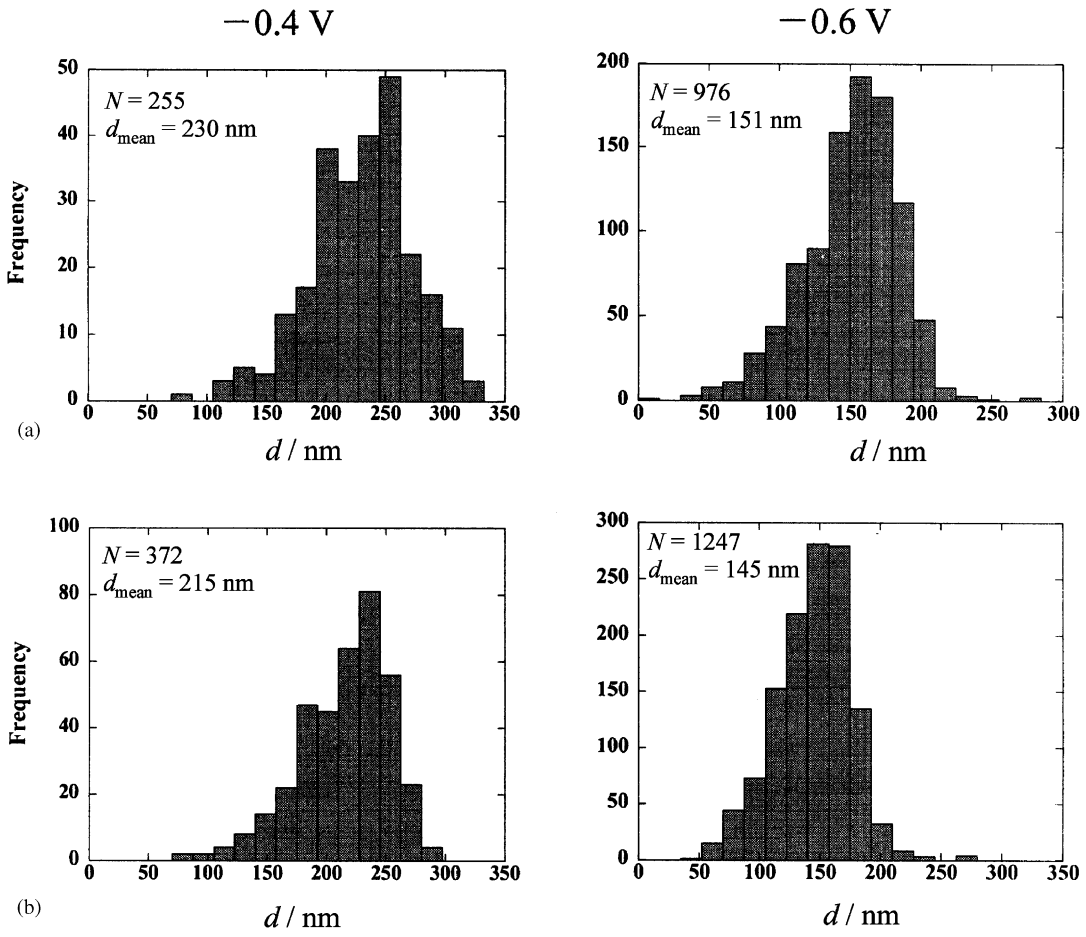

Fig. 5. Particles size distributions for the images shown in Fig. 3.

Stage III must be related directly to Bernard convection. Thus, the surface concentration of Cu^{2+} ion is maintained at a higher level than that in Stage III in the C/A configuration, for at least 10 s after starting the electrolysis. If the nuclei number density were determined primarily by the surface concentration of Cu^{2+} ions at the substrate, a greater number of nuclei would be introduced in Stage III, accompanying Bernard convection. The SEM pictures, however, demonstrate that the dependence of nucleus density on the gravitational strength clearly appears at a much earlier stage.

3.3. The distribution over the surface

Why was a higher nucleus density obtained in the potentiostatic electrodeposition in the C/A configuration than in A/C? The ionic mass transfer rate of Cu^{2+} ion should inevitably participate in the nucleation related phenomena, because it is easily influenced by the gravitational strength. The coupling phenomena between the ionic mass transfer rate and the shape of the evolution phenomena have to be understood quantitatively. Many physicists and colloid chemists have been fascinated by this topic, because such phenomena are involved in a wide variety of fractal structures as randomly deposited particles diffuse and aggregate.

Aizenberg et al. reported a method to control the crystal nucleation by patterned self-assembled monolayers [21]. The nucleation number density of calcite was successfully controlled on a metal substrate patterned with a self-assembled monolayer having areas of different nucleating activity in calcium chloride solution and the concept of an "inhibited" zone around the nucleus was discussed [21]. In surface growth models, the regime in which diffusion–controlled aggregation and growth occurs on the surface with predeposited islands is usually referred to as submonolayer, or island, epitaxy [22,23]. A DDA (deposition, diffusion and aggregation) model has proposed the characteristic length scale for a diffusion-limited, island-specific epitaxy behavior: the inhibition zone length l_d that defines the size of the region where deposition does not occur, l_d(diffusivity/flux of particles)$^{1/4}$.

Milchev and co-workers [24–29] and Scharifker and co-workers [30,31] similarly assumed that the diffusion field growing around nuclei plays an important role in determining the kinetics of the early stages of electrodeposition; both nucleation and growth rates are

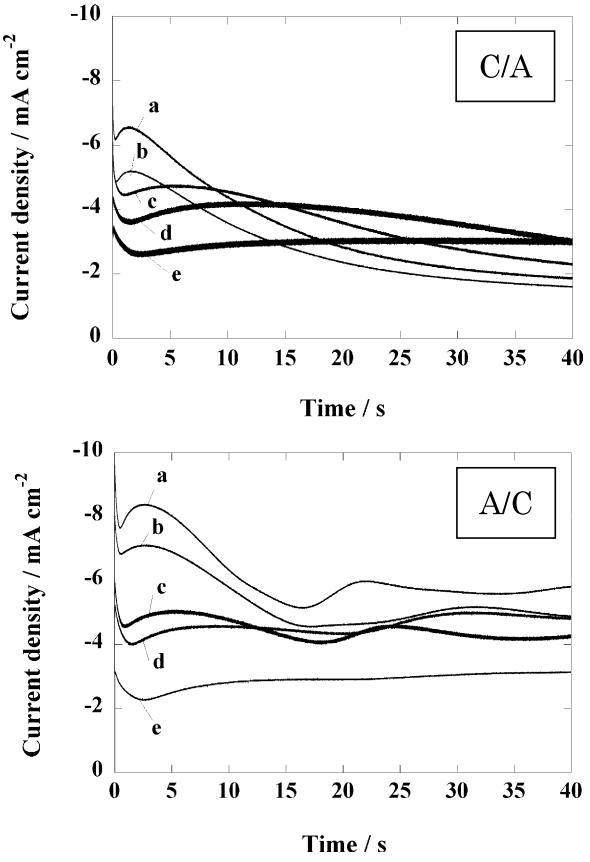

Fig. 6. Current transients for the deposition of copper in (top) the C/A configuration and (bottom) the A/C configuration. The potential was stepped from the open-circuit potential to (a) −0.7, (b) −0.6, (c) −0.5, (d) −0.4, and (e) −0.3 V.

affected by the presence of a region with reduced supersaturation around established nuclei centers. This phenomenon contributes to the progressive decay of the nucleation rate. The propagation of a nucleation-inhibited zone thus affects the spatial distribution of nuclei on the electrode surface. Stochastic analysis has been applied to discuss the nearest-neighbor distribution function. The effect of gravitational strength on the nucleus number density may be partly understood by taking into account the interaction of inhibition.

In this section, the spatial distribution relating to the inhibited zone around nucleus will be examined based on good reproducibility of the nucleation phenomena. Many kinds of single-crystal electrodes have often shown inhomogeneous nucleation phenomena (see figure 8 of Ref. [32]). The uniform distribution of surface defects over a TiN substrate must first be confirmed in order to distinguish the inhibited zone effect from the originally existing surface sites with energetic inhomogeneity.

The space distribution of nucleus events was analyzed with a typical statistical technique proposed by Budevski et al. [33]. The 8.13×8.13 μm SEM image in Fig. 3 was divided into 2000×2000 unit segments. The center coordinates of each precipitate at −0.4 V in A/C were determined in a non-dimensional system. The origin of the x–y coordinate system was placed in the lower left corner of the image. The spatial distribution looks random, suggesting an absence of preferred nucleation sites over the substrate. A random distribution mode would require a linear increase in the cumulative probability of the independent occurrence of nucleation sites in space segments along one of the directions, x or y, respectively. A typical example is shown in Fig. 7 (a). The deviation from the cumulative probability function is plotted as the residuals in Fig. 7 (b) as a function of the coordinate x or y respectively. All residuals lie within the 95% confidence level for a random distribution mode. Even for the other electrolytic conditions, they are also within the 95% limit. These results indicate that there is no maldistribution of copper precipitates on TiN substrate. This is significantly different from the case of copper electrodeposited along a rolling crack on a polycrystalline Cu substrate [12].

Next, the spatial correlations between nuclei were examined by applying a similar technique by Radisic et

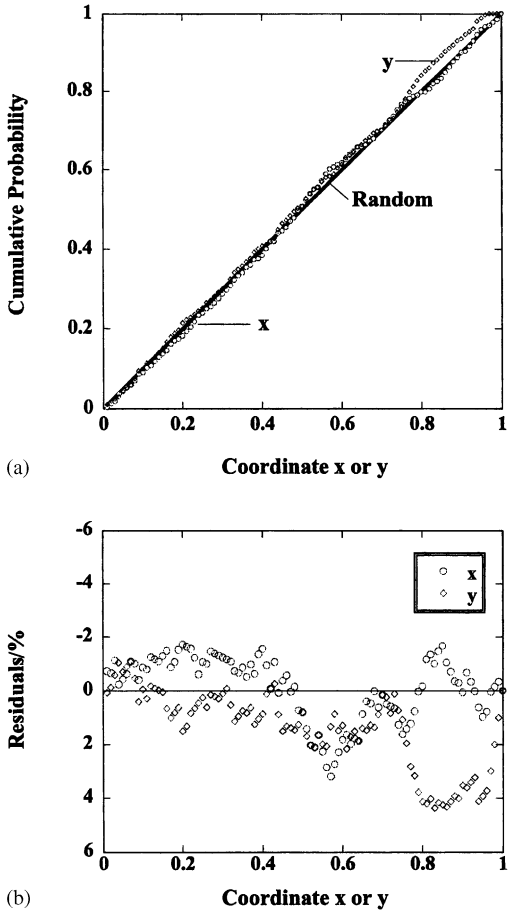

Fig. 7. (a) Cumulative probability distributions for occurrence of the nucleation coordinate along one of the coordinates, x or y, respectively. (b) Residuals of the cumulative probability distribution of the nucleation coordinates of graph (a).

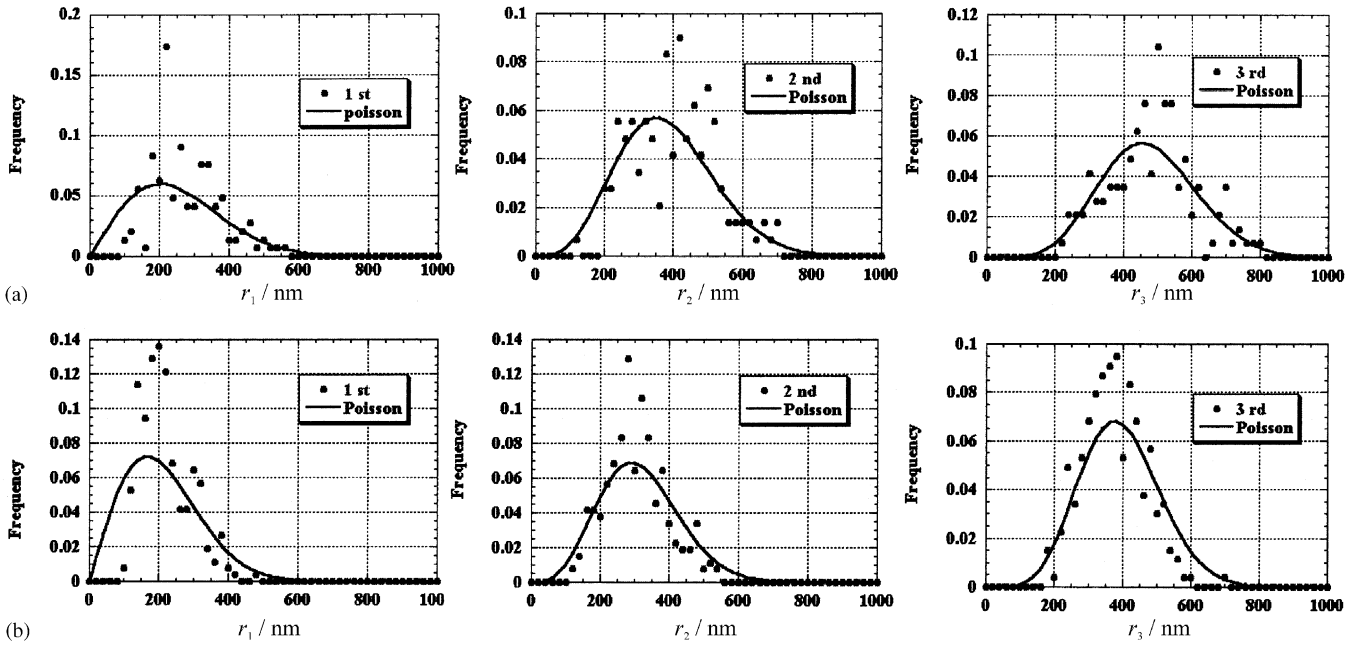

Fig. 8. Probability distribution for the first, second and third near-neighbor distance obtained in 8.14 × 8.14 μm SEM images for a charge of 31.8 mC cm^{-2} at −0.4 V. (a) C/A configuration and (b) A/C configuration. The solid line shows Poisson distribution.

al. [34], Milchev and co-workers [24–29] and Scharifker and co-workers [30,31]. Fig. 8 shows the probability distribution functions of the measured distances r_1, r_2, and r_3 between the focused nucleus and the first, second and third neighbours, respectively. The data were obtained for a copper sample electrodeposited for 31.8 mC cm^{-2} at −0.4 V under the C/A and A/C configurations. Only nuclei located at a distance larger than $2r_3$* from the edge of the SEM picutures were taken into consideration in order exclude the edge effects.

The probability of the jth-neighbour for Poisson distribution function is formulated by [35]

$$dP(r_j) = \frac{2}{(j-1)!}(\pi N_0)^j r_j^{2j-1}\exp(-\pi r_j^2 N_0)dr_j \quad (1)$$

where N_0 is the nuclei density and r_j is the distance between the jth-neighbour nuclei. The solid line in Fig. 8 corresponds to Eq. (1) with the measured nuclei density $N_0 = 1.35 \times 10^9$ cm^{-2} in C/A and $N_0 = 1.87 \times 10^9$ cm^{-2} in the A/C configuration. For Poisson distribution, the average jth distances to the first r_1*, second r_2*, third neighbors r_3*, and their standard deviations σ_j are easily fomulated in Table 1. These parameters expected from the measured number N_0 are shown in Table 2.

Table 1
r_j *, σ_j, and σ_j/r_j* for Poisson spatial distributions of the first, second and third nearest neighbors

j	r_j*	σ_j	σ_j/r_i*
1	$1/(2N_s^{1/2})$	$[(4-\pi)/4\pi N_s]^{1/2}$	0.523
2	$3/(4N_s^{1/2})$	$[(32-9\pi)/16\pi N_s]^{1/2}$	0.364
3	$15/(16N_s^{1/2})$	$[(768-225\pi)/256\pi N_s]^{1/2}$	0.295

The application of image processing makes it possible to analyze the inter-particle distances in the SEM pictures directly to calculate these parameters. Table 3 demonstrates these parameters obtained at −0.4, −0.5, and −0.6 V on C/A and A/C configurations. Comparing these parameters in Table 3 with those from the theoretical Poisson distribution functions listed in Table 2 demonstrates that the first neigbour distance r_1* is much larger than those in Poisson distribution and that the measured distribution function is slightly shifted towards longer distance. These results surely demonstrate the presence of the inhibited or exclusion zone around the growing nuclei.

The spatial distribution induced by the actual nucleation mechanism is thus characterized by these measured parameters. The difference of mean distances r_j* between the A/C and C/A configuration represents the degree of influence of the inhibition zone on the nucleation phenomena. The smaller mean distance r_i* should correspond to the smaller radii of the inhibition zone l_d. Consequently, the growth rate of the diffusion layer around the growing nucleus is smaller in A/C than in C/A. The reasons why such a difference of the propagation rate of diffusion layer is introduced in the different cell configurations, may be understood from the ionic mass transfer rate difference, that is, the flux or surface diffusivity difference, probably caused by microscopic electrolyte convection among aggregates or precipitates.

Table 2
r_j* and σ_j corresponding to measured distributions

	η/V	$10^{-8}N$/cm^{-2}	r_1*/nm	r_2*/nm	r_3*/nm	σ_1/nm	σ_2/nm	σ_3/nm
C/A	−0.4	3.53	285.84	416.56	500.55	98.37	132.32	137.86
	−0.5	6.77	247.59	313.40	376.92	65.38	78.60	81.90
	−0.6	13.5	157.49	208.50	252.00	41.74	53.90	56.21
A/C	−0.4	5.62	228.06	310.10	383.22	69.39	90.18	92.34
	−0.5	10.2	181.21	231.29	279.42	46.82	58.70	64.10
	−0.6	18.7	141.82	182.13	222.16	38.64	49.08	53.55

Table 3
Analytical values of r_j* and σ_j obtained from equations listed in Table 1 using experimental N_0 data

	η/V	$10^{-8}N$/cm^{-2}	r_1*/nm	r_2*/nm	r_3*/nm	σ_1/nm	σ_2/nm	σ_3/nm
C/A	−0.4	3.53	266.12	399.18	498.98	139.11	144.90	146.75
	−0.5	6.77	192.17	288.25	360.31	100.45	104.63	105.97
	−0.6	13.5	136.05	204.14	255.16	71.13	74.10	75.04
A/C	−0.4	5.62	210.91	316.37	395.46	110.25	114.84	116.31
	−0.5	10.2	156.56	234.83	293.54	81.84	85.24	86.33
	−0.6	18.7	115.62	173.44	216.80	60.44	62.96	63.76

4. Summary

Copper was electrodeposited potentiostatically for 31.8 mC cm^{-2} on a sputtered TiN substrate. The present technique made it possible to distinguish the metal nucleus from the substrate and to determine the nucleus number density. Thus, TiN film is a good candidate for the substrate. Two kinds of electrolytic cell configuration of cathode over anode and anode over cathode were employed. The nucleus number density was higher in the A/C than in the C/A configuration. Moreover, the statistical analysis on the mutual distance between the nuclei indicates that Cu^{2+} ion does not precipitate randomly on TiN substrate and that the deviations from Poisson distribution are ascribed to the presence of nucleation inhibited zones. The inhibited zone length in C/A is larger than that in A/C. The influence of gravitational strength to the growing inhibited zone must be further analyzed.

References

[1] J. St. Pierre, N.Y. Jia, J. New Mat. Electr. Sys. 5 (2002) 263.
[2] G.J.K. Acres, J. Power Sources 100 (2001) 60.
[3] Y. Sone, M. Ueno, S. Kuwajima, Electrochemistry 70 (2002) 705.
[4] R. Raffaelle, J. Maranchi, P. Kumta, D. Scheiman, M. Khan, A. Hepp, Abs. Papers Am. Chem. Soc. 222 (2001) 360.
[5] S.G. Baily, R. Raffaelle, K. Emery, Prog. Photovoltaics 10 (2002) 399.
[6] G. Halpert, H. Frank, S. Surampudi, Interface Fall (1999) 25.
[7] W. Wopersnow, Ch.J. Raub, Z. Flugwiss. Weltraumforsch 2 (1978) 341.
[8] V.G. Nefedov, V.M. Serebritskii, O.S. Ksenzhek, V.P. Nikiskii, M.B. Bocharova, A.N. Balandin, A.Y. Solovev, Russian J. Electrochem. 30 (1994) 1229.
[9] H. Kaneko, K. Tanaka, A. Iwasaki, Y. Abe, M. Kamimoto, Electrochim. Acta 43 (1993) 729.
[10] A. Iwasaki, H. Kaneko, Y. Abe, M. Kamimoto, Electrochim. Acta 43 (1998) 509.
[11] T. Mori, K. Goto, R. Ohashi, A. Sawaoka, Microgravity Sci. Technol. 5 (1993) 238.
[12] Y. Fukunaka, K. Okano, Y. Tomii, Z. Asaki, K. Kuribayashi, J. Electrochem. Soc. 145 (1876) 1998.
[13] K. Okano, Master Thesis, Kyoto University, 1995.
[14] Y. Konishi, Ph. D., Dissertation, Kyoto University, 2001.
[15] Y. Fukunaka, Y. Kondo, Electrochim. Acta 26 (1981) 1537.
[16] J.G. Ryan, R.M. Geffken, N.R. Poulin, J.R. Paraszczak, IBM J. Res. Develop. 39 (1995) 371.
[17] T.J. Licata, E.G. Colgan, J.M.E. Harper, S.E. Luce, IBM J. Res. Develop. 39 (1995) 419.
[18] V. Fleury, J.H. Kaufman, D.B. Hibbert, Nature 367 (1994) 435.
[19] M. Wang, W.J.P. van Enckevort, N.-b. Ming, P. Bennema, Nature 367 (1994) 438.
[20] D.G. Grier, D. Mueth, Phys. Rev. E 48 (1993) 3841.
[21] J. Aizenberg, A.J. Black, G.M. Whitesides, Nature 398 (1999) 495.
[22] P. Jensen, Al. Barabasi, H. Larralde, S. Havlin, H.E. Stanley, Phys. Rev. E 50 (1994) 618.
[23] P. Jensen, Al. Barabasi, H. Larralde, S. Havlin, H.E. Stanley, Phys. Rev. B 50 (1994) 15316.
[24] A. Milchev, J. Electroanal. Chem. 312 (1991) 267.
[25] A. Milchev, Electrochim. Acta 37 (1992) 2229.
[26] E. Michilova, A. Milchev, Electrochim. Acta 37 (1992) 2233.
[27] A. Milchev, W.S. Kruijit, M. Sluyters-Rehbach, J.H. Sluyters, J. Electroanal. Chem. 362 (1993) 21.
[28] W.S. Kruijit, M. Sluyters-Rehbach, J.H. Sluyters, A. Milchev, J. Electroanal. Chem. 371 (1994) 13.

[29] A. Milchev, E. Michailova, I. Lesigiarska, Electrochem. Commun. 2 (2000) 407.
[30] E. Garcia-Pastoriza, J. Mostany, B.R. Scharifker, J. Electroanal Chem. 441 (1998) 13.
[31] A. Serruya, J. Mostany, B.R. Scharifker, J. Electroanal. Chem. 464 (1999) 39.
[32] A. Milchev, Electrochim. Acta 28 (1983) 947.
[33] E. Budeuvski, G. Staikov, W.J. Lorenz, Electrochemical Phase Formation and Growth—An Introduction to the Initial Stage of Metal Deposition, VHC, Weinheim, 1996.
[34] A. Radisc, J.G. Lomg, P.M. Hoffmann, P.C. Searson, J. Electrochem. Soc. 148 (2001) C41.
[35] A. Milchev, W.S. Kruijt, M. Sluyters-Rehbach, J.H. Sluyters, J. Electroanal. Chem. 350 (1993) 89.